



# First Beam Kick Measurements in the PETS

Roger Ruber and Volker Ziemann  
Department of Physics and Astronomy  
Uppsala University, Sweden

Erik Adli  
University of Oslo, Norway

## Abstract

We present the results of beam kick measurements in the PETS during the first commissioning phase in December 2008. The measurements have shown no correlation between beam kick and beam position or power production in the PETS. A method is proposed to improve the kick measurements by taking into account the incoming beam's energy.

Geneva, Switzerland

December 3, 2009

# 1 Introduction

The power generation structures (PETS) for CLIC are presently tested [1, 2, 3] in the Two-beam Test Stand (TBTS) which is part of the CTF3 accelerator test facility at CERN. Here a high intensity electron beam passes through the PETS structure generating 12 GHz RF power. Both electron beam parameters and the generated RF power are recorded with fast oscilloscopes. The PETS structure is equipped with a RF recirculation mechanism that allows to feed back part of the generated power to the input in order to increase the intra-PETS power level. A schematic of the set-up is shown in figure 1.

In previous notes we have described the analysis of the measured RF power [4, 5, 6]. In this note we describe the beam kick measurements based on the techniques described in note [8]. With the beam position monitors (BPM) located before and after the PETS it is possible to measure the incoming and outgoing beam position and angle. The BPM after the spectrometer bending magnet can be used to monitor changes in the beam energy. Thus the BPMs can be used to monitor beam kicks and energy loss inside the PETS. The beam energy loss estimation have been described in a previous note [7].

## 2 Analytical Beam Kick Estimation

The kick  $\theta \equiv \Delta x'$  an electron inside the PETS receives due to the dipole wake caused by the offset  $x_P(s)$  of a leading particle can be estimated by integrating the force over the PETS length

$$\theta = \int_0^{L_{\text{PETS}}} ds \frac{x_P(s)}{E_{\text{tot}}} eq_1 W_T(z). \quad (1)$$

We assume a 12 GHz bunch train with an intensity of  $I = 5 \text{ A}$  and a beam energy  $E_{\text{tot}} = 127 \text{ MeV}$ . For a PETS without damping material the dipole wake can then be approximated as a single mode with parameters  $2k'_T \approx 8.3 \text{ V/pC/m/mm}$ ,  $Q \approx 5000$ , mode frequency  $f_T \approx 15 \text{ GHz}$  and a group velocity  $\beta \approx 0.7$ , but bouncing forth and back inside the cavity. If we assume a worst case scenario of zero group velocity, the maximum kick due to a leading

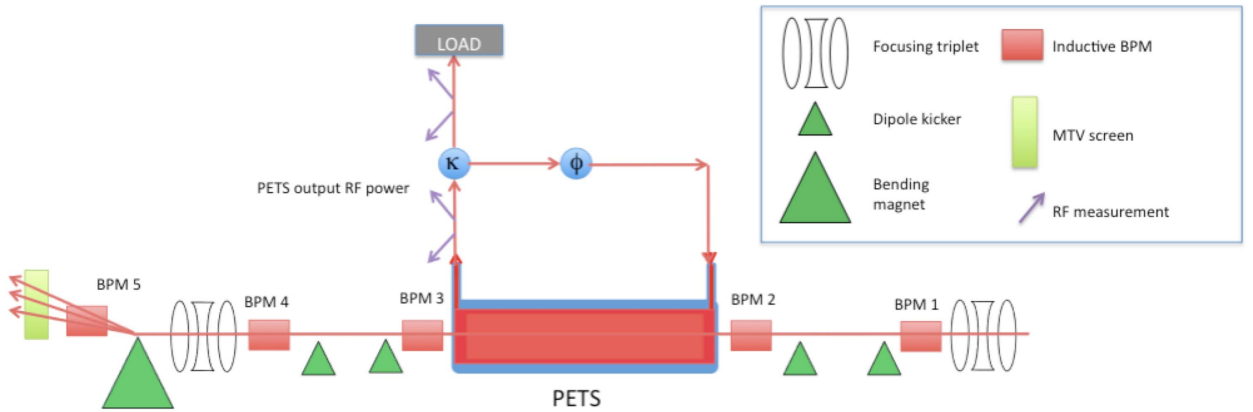


Figure 1: Set-up of the TBTS drive beam with PETS and recirculation mechanism. The beam enters the set up from the right.

bunch on a trailing bunch is estimated as

$$\theta/x_P = 2 \frac{L_{\text{PETS}}}{E_{\text{tot}}} e \frac{I}{f_{\text{bunch}}} k'_T = 27 \mu\text{rad}/\text{mm} \quad (2)$$

with a PETS length  $L_{\text{PETS}} = 1$  m and  $x_P$  given in [mm] [9]. The order of magnitude of the kick does not depend strongly on the frequency as long as it is far from a multiple of the bunch frequency of 12 GHz.

### 3 Kick and Energy Loss Determination

A beam kick inside the PETS can be determined using the horizontal and vertical beam position measurements in the BPMs. This technique is described in detail in [8]. The five BPMs in the beam line (figure 1) measure the respective beam positions  $x_1, x_2, x_3, x_4, x_5$ . The two BPMs upstream of the PETS determine the incoming beam's position offset  $x$  and angle  $x'$ . And the two BPMs downstream of the PETS then determine the outgoing beam kick angle  $\theta$ . The fifth BPM after the spectrometer bending dipole resolves the relative beam energy change  $\delta$ .

The beam position at the 5 BPMs is given by [8]

$$\begin{pmatrix} x_1 \\ x_2 \\ x_3 \\ x_4 \\ x_5 \end{pmatrix} = \begin{pmatrix} 1 & 0 & 0 & 0 \\ R_{11}^{21} & R_{12}^{21} & 0 & 0 \\ R_{11}^{31} & R_{12}^{31} & R_{12}^{3K} & 0 \\ R_{11}^{41} & R_{12}^{41} & R_{12}^{4K} & 0 \\ R_{11}^{51} & R_{12}^{51} & R_{12}^{5K} & R_{16}^{5K} \end{pmatrix} \begin{pmatrix} x_1 \\ x'_1 \\ \theta_x \\ \delta_x \end{pmatrix} = \mathbf{A} \begin{pmatrix} x_1 \\ x'_1 \\ \theta_x \\ \delta_x \end{pmatrix} \quad (3)$$

where  $K$  indicated the longitudinal position of the beam kick. The least squares estimation of the beam kick and energy loss from these 5 BPM signals is then given by

$$\begin{pmatrix} x_1 \\ x'_1 \\ \theta_x \\ \delta_x \end{pmatrix} = (\mathbf{A}^T \mathbf{A})^{-1} \mathbf{A}^T \begin{pmatrix} x_1 \\ x_2 \\ x_3 \\ x_4 \\ x_5 \end{pmatrix} \quad (4)$$

for which the covariance  $\Sigma$  is determined by the accuracy  $\sigma$  of the BPM readings:

$$\Sigma = (\mathbf{A}^T \mathbf{A})^{-1} \sigma_{\text{BPM}}^2. \quad (5)$$

Note that the derived relative beam energy change can be caused by the PETS or beam kick but can also be due to variations in the incoming beam's energy. The incoming beam's energy variation can also lead to a misinterpretation of the derived kick angle  $\theta$ . This could be verified by measuring the incoming beam's energy variation with help of a "dog-leg" upstream of the PETS, see appendix A, but the data required was not yet included for the 2008 measurements.

The relative beam energy change measurement with the fifth BPM and bending dipole only works in the horizontal plane. Thus for the vertical plane the matrix  $\mathbf{A}$  is simplified to

a four by three matrix

$$\begin{pmatrix} y_1 \\ y_2 \\ y_3 \\ y_4 \end{pmatrix} = \begin{pmatrix} 1 & 0 & 0 \\ R_{11}^{21} & R_{12}^{21} & 0 \\ R_{11}^{31} & R_{12}^{31} & R_{12}^{3K} \\ R_{11}^{41} & R_{12}^{41} & R_{12}^{4K} \end{pmatrix} \begin{pmatrix} y_1 \\ y_1' \\ \theta_y \end{pmatrix} = \mathbf{A}_y \begin{pmatrix} y_1 \\ y_1' \\ \theta_y \end{pmatrix}. \quad (6)$$

## 4 Transfer Matrices

The horizontal transfer matrix  $A = A_x$ , as defined in section 3, depends upon the settings of the quadrupole magnets while the vertical transfer matrix  $A_y$  does not. The vertical transfer matrix  $A_y$  does neither have the 5th row as there is no bending in the vertical plane between BPM 4 and BPM 5. The transfer matrices are prepared from the beam line description lattice by MAD-X [10] based on the BPM positions as given in [11]. For the 11 December 2008 measurements, they become:

$$A_x = \begin{pmatrix} 1 & 0 & 0 & 0 \\ 1 & 1.5703 & 0 & 0 \\ 1 & 4.0786 & 1.2787 & 0 \\ 1 & 6.1000 & 3.3000 & 0 \\ -0.5391 & -1.3539 & 0.1556 & -0.2325 \end{pmatrix} \quad (7)$$

$$A_y = \begin{pmatrix} 1 & 0 & 0 \\ 1 & 1.5703 & 0 \\ 1 & 4.0786 & 1.2787 \\ 1 & 6.1000 & 3.3000 \end{pmatrix}. \quad (8)$$

The accuracy of the beam kick estimation is a static parameter determined by the transfer matrices and the resolution of the BPM based position measurement as given in equation 5. With a BPM resolution  $\sigma = 10 \mu\text{m}$ , the accuracy of the kick estimation becomes

$$\sigma(x_1) = \sigma(y_1) = \sqrt{\Sigma_{11}} = 9.5 \mu\text{m} \quad (9)$$

$$\sigma(x_1') = \sigma(y_1') = \sqrt{\Sigma_{22}} = 6.5 \mu\text{m} \quad (10)$$

$$\sigma(\theta) = \sqrt{\Sigma_{33}} = 11.2 \mu\text{rad} \quad (11)$$

$$\sigma(\delta) = \sqrt{\Sigma_{44}} = 0.542 \times 10^{-3} \quad (12)$$

Thus with our set-up it should be possible to measure the beam kick as the accuracy for the beam kick estimation is a factor two smaller than the estimated beam kick  $27 \mu\text{rad}/x_P$  (equation 2).

## 5 Data Analysis Software

A set of MATLAB [12] functions has been prepared for the analysis of the measured beam pulses. They load, process and display the data from the BPM and RF measurements and are described in appendix B. The analyses of the beam kick according to the method described in section 3 is integrated in this software. The transfer matrices for the beam kick estimation are based on the actual magnet current settings according the log book.

The transfer matrices  $A_x$  and  $A_y$  are named **BX** and **BY** respectively and calculated from a MAD-X [10] lattice file `tbts_db.lat`:

```
[BX,BY] = tbts_lattice_calculation( 'tbts_db.lat', lupdate );
```

The structure `lupdate` contains the actual current settings of the quadrupole magnets. Both transfer matrices are calculated as  $5 \times 4$  matrices, but for `BY` only a  $4 \times 3$  size is used in the subsequent calculations. Based on these matrices, the beam kick  $\theta$  is calculated as

```
for ibpm = 1:5
    dposx(ibpm) = bpmdatx(ibpm,k);
    dposy(ibpm) = bpmdatay(ibpm,k);
end
dposy(5) = [];
theta_x(k,:) = BX\dposx';
theta_y(k,:) = BY\dposy';
```

Assuming a BPM resolution of  $10 \mu\text{m}$ , the covariance for the fitted parameters is calculated as

```
rmseerror = 0.010;
covx = rmseerror*sqrt(diag(inv(BX'*BX)));
covy = rmseerror*sqrt(diag(inv(BY'*BY)));
```

## 6 Measurement Data and Discussion

With the tools explained in sections 3 and 5 it is now possible to analyze the event data and calculate the beam kick inside the PETS. Based on equation 2 we investigate the relation between the beam kick and the beam offset and current. We also look at a possible effect of a RF breakdown. The pulses discussed in this section are from the 11 December 2008 run. Their numbering is according to the series as defined in appendix C of [6]. The beam energy during this run was 127 MeV [7]. During the data taking all orbit corrector magnets were switched off with exception of CM.DVJ0340 (-1.00 A) and CM.DVJ0520 (0.30 A). These are the vertical orbit correctors behind our BPMs number 1 and 3 respectively (figure 1).

Appendix C contains plots of a set of measured pulses, some of which display pulse shortening (4-1, 4-2, 7-361, 7-455 and 7-517) and some not (7-1, 7-2, 7-150 and 7-394). The RF power of the pulses is measured with 12 GHz diodes. The measured RF power is compared to the power reconstructed from the beam intensity according the procedure described in [4]. The BPM 2 (CM.BPM 0370) just upstream of the PETS is used for this reconstruction with gain 0.75 and phase shift  $18^\circ$  as determined in [6]. Pulse 4-1 and 7-150 both have a somewhat similar shape for the beam current and equal maximum power output level. However, around 170 ns from the start of the beam pulse, pulse 4-1 displays pulse shortening behaviour. We assume this to correspond to a RF breakdown, possibly but not necessary inside the PETS. The flat top of the beam current is considered to be the period between 100 and 300 ns.

First we will look at pulse 7-150 in detail with help of the plots in appendix D. Figure 16(b) shows the horizontal and vertical position and angle of the incoming beam as measured at the first BPM and extrapolated to the centre of the PETS. The beam position and angle at the PETS centre are calculated from the data at BPM 2 and 3 assuming no beam kick and thus a straight line between these two BPMs. Of course, as we want to estimate the beam kick inside the PETS this condition can not be assumed true, but based

on the analytical estimation of the kick as given by equation 2, it can be assumed small in first order. This gives an estimation of the average beam position inside the PETS. The off-axis horizontal beam position and angle at the PETS centre are within 1 mm and 1 mrad offset respectively. The vertical beam angle is also around 1 mrad, but the vertical offset is around 7 to 7.5 mm.

Figure 16(c) shows estimated horizontal and vertical beam kicks. The horizontal kick is smaller than -0.5 mrad for a horizontal beam position offset of 0 to 0.5 mm. The vertical kick is of the same order, but the signal displays more noise due to noise in the BPM measurements. The estimated horizontal kick angle is rather smooth compared to the vertical one, due to the input data, but both seem to have a small peak roughly every 30 ns. This oscillation originates from a 30 ns period in the analogue memory used by the BPM signal digitizers which is running at a frequency of 96/3 MHz. The same figure also shows the relative energy change of the beam. Note that this plot has a minimum around 200 ns, which corresponds to the maximum in the RF power production.

Figure 17(a) contains scatter plots of the kick angle against the beam position and angle at the PETS centre. It shows the correlation between the horizontal kick angle and horizontal beam position or angle, and between the vertical kick angle and the vertical beam position or angle. Only the data from measurement points within the beam current flat top has been plotted. There is no obvious correlation between the data points.

Figure 17(b) shows scatter plots of the horizontal and vertical kick angle against the beam current intensity and the PETS RF output power. Also for these plots only the data within the beam current flat top has been used. A straight line has been fitted through the data points of the horizontal kick angle. Although there is a large spread in the data points, there seems to be some correlation between the horizontal kick angle and the beam intensity and PETS RF output power (which is related to the square of the beam intensity). A straight line has been fitted through these data sets. There is no obvious correlation for the vertical kick angle.

Finally, the left hand side of figure 17(c) shows scatter plots of the horizontal and vertical kick angle versus the energy loss  $\Delta E$ . Also here is a correlation visible for the horizontal kick angle versus beam momentum loss, but not for the vertical kick angle. The right hand side of figure 17(c) shows a scatter plot of the beam position versus the beam energy loss with some correlation between the data points for the horizontal beam position.

For the correlation between beam position and beam energy loss we should remember that the beam energy loss is in fact the relative change in energy as function of time along the beam pulse. The measured relative beam energy change can be caused by the PETS but also by variations in the incoming beam's energy. And, as the beam passes several dipole magnets before arrival in the TBTS PETS, as a consequence there will be variations in the incoming beam's position. As can be seen from the plots in figure 7(b), the beam position at BPM 1 and the PETS centre is not constant along the pulse. Therefore the correlation between beam position and beam energy "loss" is likely due to variations in the incoming beam's energy.

Figures 18 and 19 repeat the same correlation plots but with the data points selected from the first halve of the beam current flat top (100 to 200 ns) and the second halve (200 to 300 ns) respectively. The same correlations are visible, and in figure 18 also between horizontal kick angle and horizontal position while in figure 19 there is no longer a clear correlation to the RF power visible.

For pulse 4-1, the beam position at the PETS centre and the estimated kick are shown in figure 12. This pulse is vertically better centred than pulse 7-150. Note however that position and angle show more variation over the flat top which is, like in pulse 7-150, from 100 to 300 ns. Note also that the horizontal kick angle seems to be constant during the flat top while the vertical kick angle decreases by almost 2.5 mrad.

Figure 13 shows scatter plots of the pulse's flat top data for horizontal and vertical kick angle and beam position at the left and the kick angle and beam current on the right hand side. No clear relation is visible in any of the plots except for the beam position versus beam energy loss in the right hand side of (c). Figure 14 and 15 show the same correlation plots, but the data is split for the period 100 to 200 ns and the period 200 to 300 ns respectively. The split around 200 ns corresponds roughly to the start of the pulse shortening. In figure 14 a correlation is visible between the horizontal kick angle and beam position, current, RF power and energy loss, but not for the beam position with respect to the beam energy loss. The correlations are not visible in the second part of the pulse as shown in figure 15, except for the beam position versus beam energy loss which now has a clear correlation.

The plots in appendix C show for the selected pulses a plot of the RF power, beam current, kick angle and energy loss as function of time. In addition scatter plots are shown of the kick angle versus beam position and of the kick angle versus energy loss. For several of the pulses there is a correlation visible for the horizontal kick angle. However, none of the pulses displays any correlation behaviour for the vertical kick angle. Therefore we believe that the correlation between horizontal kick angle and horizontal beam position is related to the variation of the incoming beam's energy.

In addition all of the pulses display a build-up of the reflected power during the pulse. The reflected power is not linear related to neither the forward power or the power into the load. Combined with the conclusions from [13] this indicates that the pulse shortening behaviour is not due to breakdown inside the PETS but rather to activity inside the recirculation loop.

## 7 Conclusions

We have deduced and tested a method to measure the beam kick angle inside the PETS. Measurements show some correlation between beam kick angle and beam position but this is likely due to a correlation between the incoming beam's position and beam energy variations. The correlation behaviour is similar for pulses with and without pulse shortening and shows only for the horizontal kick, not for the vertical, an effect of the horizontal bending dipoles upstream of the PETS. The experimental method will be improved by including an energy measurement of the incoming beam.

Our method seems to be limited by noise on the beam position measurement signals. Furthermore the relative alignment between BPMs and PETS should be verified by measuring the kick angle for different beam offsets inside the PETS with a zero incoming beam angle.

## References

- [1] I.Syratchev, G. Riddone and S. Tantawi, *CLIC RF High Power Production Testing Program*, Proc. of the EPAC'08, Genoa, June 2008.

- [2] I. Syratchev, *PETS and drive beam development for CLIC*, Proc. of the 44th ICFA Advanced Beam Dynamics Workshop, X-band RF Structure and Beam Dynamics, Daresbury, December 2008.
- [3] E. Adli et al., *First Results of the CLIC Power Extraction Structure in the Two-beam Test Stand*, Proc. of the DIPAC'09, Basel, May 2009.
- [4] R. Ruber and V. Ziemann, *An Analytical Model for PETS Recirculation*, CERN CTF3 Note 92 (2009).
- [5] V. Ziemann, *Data Analysis for PETS Recirculation*, CERN CTF3 Note 94 (2009).
- [6] E. Adli, *Analysis of the first 12 GHz PETS tests with beam using a constant parameter recirculation model*, CERN CTF3 Note 96 (2009).
- [7] E. Adli, *Techniques for estimations of beam energy loss in the Two-beam Test Stand PETS, applied to the first 12 GHz PETS tests with beam*, CERN CTF3 Note 97 (2009).
- [8] M. Johnson, *Beam-based Diagnostics of RF-breakdown in the Two-beam Test Stand in CTF3*, CERN-OPEN-2007-022, CLIC note 710 (2007).
- [9] E. Adli, Ph.D. thesis, under preparation.
- [10] H. Grote and F. Schmidt, *MAD - Methodical Accelerator Design*, CERN Program Library T5001, <http://cern.ch/mad>
- [11] *MAD-X Input files for the CTF3 Two-beam Test Stand*, CERN EDMS 903028.
- [12] <http://www.mathworks.com>
- [13] C. Hellenthal, *PETS Conditioning and Breakdown Behaviour*, CERN CLIC Note 811 (2009).

## A Kick Determination with Initial Energy Variation

In reference [8] the measurements in the Two-beam Test Stand (TBTS) of CTF3 to determine the kick due to RF breakdown in the CLIC acceleration structures in the CTF3 probe-beam are described. In the meantime we apply the same method to determine the effect of the PETS structures in the drive beam. A problem in the latter case is that the incoming beam already has a large energy variation, which can lead to misinterpretations of the derived kicks. Here we will remedy this deficiency and derive the system equations to determine both the orbit  $x_1, x'_1$  and the energy variation  $\delta_1$  at BPM 1 where the geometry is described in figure 2. Moreover the kick in angle  $\theta$  and in energy  $\delta$  at the site of the breakdown on the experimental table is determined.

It is clear that we need at least one extra BPM that is separated from the other BPM already used in reference [8] (corresponding to BPM 4 to 8 in figure 2) by a dipole in order to resolve the incoming energy variation  $\delta_1$ . We see from figure 2 that in the TBTS such a BPM is actually available in the dog-leg of TL2' in the form of BPM1. We also include two additional BPM, labelled 2 and 3 which are present in TL2', even though they are not required for solving the problem, but help in yielding accuracy, due to the higher number of degrees of freedom in the fit. In fact we now have 8 measurements in the BPM and five variables to determine, namely  $x_1, x'_1, \delta_1, \theta, \delta$  where  $\delta$  is the energy variation that the beam experiences in breakdown in the PETS, and  $\delta_1$  is the energy variation of the incoming beam.

Having defined the geometry in figure 2 we are now able to write down the system matrix relating the observed positions on the BPM to the unknowns  $x_1, x'_1, \delta_1, \theta, \delta$

$$\begin{pmatrix} x_1 \\ x_2 \\ x_3 \\ x_4 \\ x_5 \\ x_6 \\ x_7 \\ x_8 \end{pmatrix} = \begin{pmatrix} 1 & 0 & 0 & 0 & 0 \\ R_{11}^{21} & R_{12}^{21} & R_{16}^{21} & 0 & 0 \\ R_{11}^{31} & R_{12}^{31} & R_{16}^{31} & 0 & 0 \\ R_{11}^{41} & R_{12}^{41} & R_{16}^{41} & 0 & 0 \\ R_{11}^{51} & R_{12}^{51} & R_{16}^{51} & 0 & 0 \\ R_{11}^{61} & R_{12}^{61} & R_{16}^{61} & R_{12}^{6K} & 0 \\ R_{11}^{71} & R_{12}^{71} & R_{16}^{71} & R_{12}^{7K} & 0 \\ R_{11}^{81} & R_{12}^{81} & R_{16}^{81} & R_{12}^{8K} & R_{16}^{8K} \end{pmatrix} \begin{pmatrix} x_1 \\ x'_1 \\ \delta_1 \\ \theta \\ \delta \end{pmatrix} \quad (13)$$

where  $R_{ij}^{kl}$  denotes the  $ij$  transfer matrix element between location labelled  $l$  and  $k$ . Just

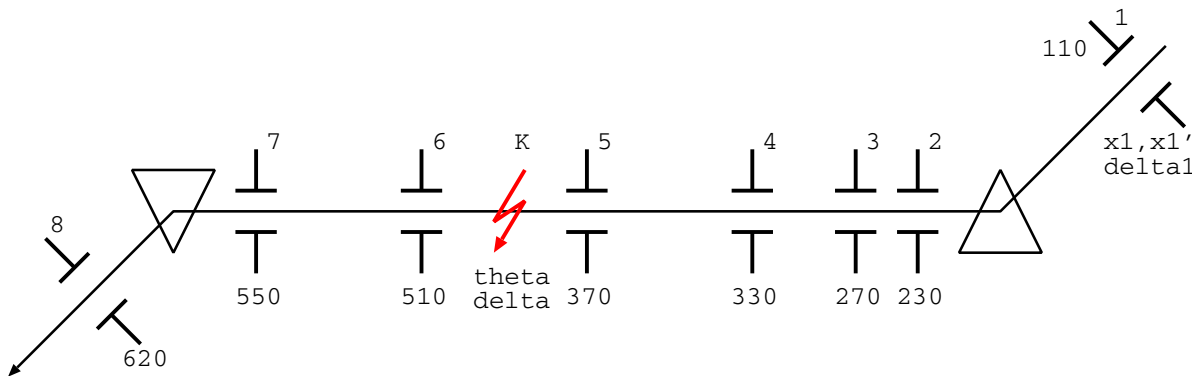


Figure 2: The geometry used for the determination of the system matrix. Note that the control system names of the BPM are also indicated for convenience.

note that we use matrix orientation from right to left, that is, the superscript denoting the start is on the right and the superscript denoting the end is on the left.

If we denote the large matrix in equation 13 by  $A$  we can solve the equation by calculating the least-square pseudo-inverse and obtain

$$\begin{pmatrix} x_1 \\ x_1' \\ \delta_1 \\ \theta \\ \delta \end{pmatrix} = (A^T A)^{-1} A^T \begin{pmatrix} x_1 \\ x_2 \\ x_3 \\ x_4 \\ x_5 \\ x_6 \\ x_7 \\ x_8 \end{pmatrix} \quad (14)$$

where  $A^T$  denotes the transpose of the matrix  $A$ . Also the covariance matrix is given by  $(A^T A)^{-1}$  and can be used to determine the error bars of the derived parameters, as already outlined in reference [8].

## B MatLAB Scripts

For the analysis of measured beam pulses we prepared a set of MatLAB functions that load, process and display the data from the BPM and RF measurements. The functions to analyse the beam kick according to the method described in section 3 are integrated in this software.

- All software is found on the CERN AFS system:

```
\afs\cern.ch\eng\cllic\tbts\upsala\matlab
```

- `pets_oasis_load.m`

loads all data from one pulse and saves it in the output structure

- `pets_oasis_calc.m`

uses the output structure from the `pets_oasis_load.m` function to

- calculate RF power and phase from the I&Q signals
- reconstruct RF power and phase from the beam intensity signal
- estimate beam kick from the beam position signals:

- `pets_oasis_plot.m`

plots results from the `pets_oasis_load.m` and `pets_oasis_calc.m` functions

- `pets_oasis_mplot.m`

plots a summary of a structure with results from multiple calls to the functions `pets_oasis_load.m` and `pets_oasis_calc.m`

These functions can be used e.g. in the following way to scan through a set pulses stored in a single folder

```
% Script: pets_oasis_ex1.m

% folder with data files
dpath = '/afs/cern.ch/eng/cllic/tbts/upsala/data/oasis';

% load the data
files = dir( dpath );
n = 0;
for k=1:size(files,1)
    if ~files(k,1).isdir
        tmp = textscan( files(k,1).name, '%s %s', 'Delimiter', '.' );
        fileName = cell2mat( tmp{1} );
        fileType = cell2mat( tmp{2} );
        if ~(strcmp(fileType,'csv') && ~strcmp(fileName(1:2),'rf'))
            n = n+1;
            x.filename = files(k,1).name;
            mpulse(n) = pets_oasis_load( x );
            mcalc(n) = pets_oasis_calc( mpulse(n) );
            y.file = ['pets' mpulse.number];
```

```

        mplot(n) = pets_oasis_plot( mpulse(n), mcalc(n), y );
    end
end
end
disp(['Processed ' num2str(n) ' files.'])

%..Plot summary
mplot = pets_oasis_mplot( mpulse, mcalc, 0 );

```

The beam kick estimation and the therefore required transfer matrices, based on the actual magnet currents, are determined in the following functions:

- `tbts_kick_pulse.m`  
makes an LSF estimation from the horizontal and vertical beam position (BPM) pulses
- `tbts_lattice_calculation.m`  
calculates the matrix **A** for the horizontal and vertical kick from a beam line description lattice prepared by MAD-X [10].  
This function is called by `tbts_kick_pulse.m`.
- `tbts_lattice_calibration.m`  
updates the beam line lattice with respect to the quadrupole strength (i.e. the actual current settings).  
This function must be called before the function `tbts_lattice_calculation.m`.  
This function is called by `tbts_kick_pulse.m`.

This is done in the following way, where **BX** and **BY** are the transfer matrices  $A_h$  and  $A_v$  respectively:

```

%% Beam kick fit over whole pulse

function [theta_x theta_y chi2x chi2y covx covy] =
    tbts_kick_pulse( bpmdatay, bpmdatay )

%..define relative magnet strenghts
lupdate = tbts_lattice_calibration( '11dec2008' );

%..calculate the system matrices
[BX,BY] = tbts_lattice_calculation( 'tbts_db.lat', lupdate );

%..use 4x3 matrix for BY as no vertical dispersion
BY(5,:) = [];
BY(:,4) = [];

%..BPM resolution of 0.010 mm
rmserror=0.010;

%..
n = length(bpmdatay);

```

```

dposx  = zeros(1,5); %..horizontal position
dposy  = zeros(1,4); %..vertical
theta_x = zeros(n,4); %..horizontal fit
theta_y = zeros(n,3); %..vertical
chi2x  = zeros(n,1); %..horizontal chi-squared error estimation
chi2y  = zeros(n,1); %..vertical

%..do the least square fit of the bpm positions to incoming orbit,
%..kick and energy change.
%..estimate the chi-squared error for each point
for k = 1:n
    for ibpm = 1:5
        dposx(ibpm) = bpmdatax(ibpm,k);
        dposy(ibpm) = bpmdatay(ibpm,k);
    end
    dposy(5) = [];
%    theta_x(k,:) = inv(BX'*BX)*BX'*dposx';
%    theta_y(k,:) = inv(BY'*BY)*BY'*dposy';
    theta_x(k,:) = BX\dposx';
    theta_y(k,:) = BY\dposy';
    fposx = BX*theta_x(k,:)' ;
    fposy = BY*theta_y(k,:)' ;
    chi2x(k) = sum( ((dposx-fposx')/rmserror).^2 );
    chi2y(k) = sum( ((dposy-fposy')/rmserror).^2 );
end

%..the error bars for the fitted parameters
covx=rmserror*sqrt(diag(inv(BX'*BX)));
covy=rmserror*sqrt(diag(inv(BY'*BY)));

```

## C Data Plots

This section contains plots of several pulses showing the PETS output RF power, beam intensity, position and kick. Correlation plots between beam kick and beam position or energy loss are also included.

Each figures includes

**Top left:** Beam current, measured RF power and reconstructed from the current.

**Top right:** Estimated beam kick and energy loss.

**Bottom left:** Beam kick versus position for the beam current flat top between 100 and 200 ns.

**Bottom right:** Beam kick versus beam energy loss for the beam current flat top between 100 and 200 ns.

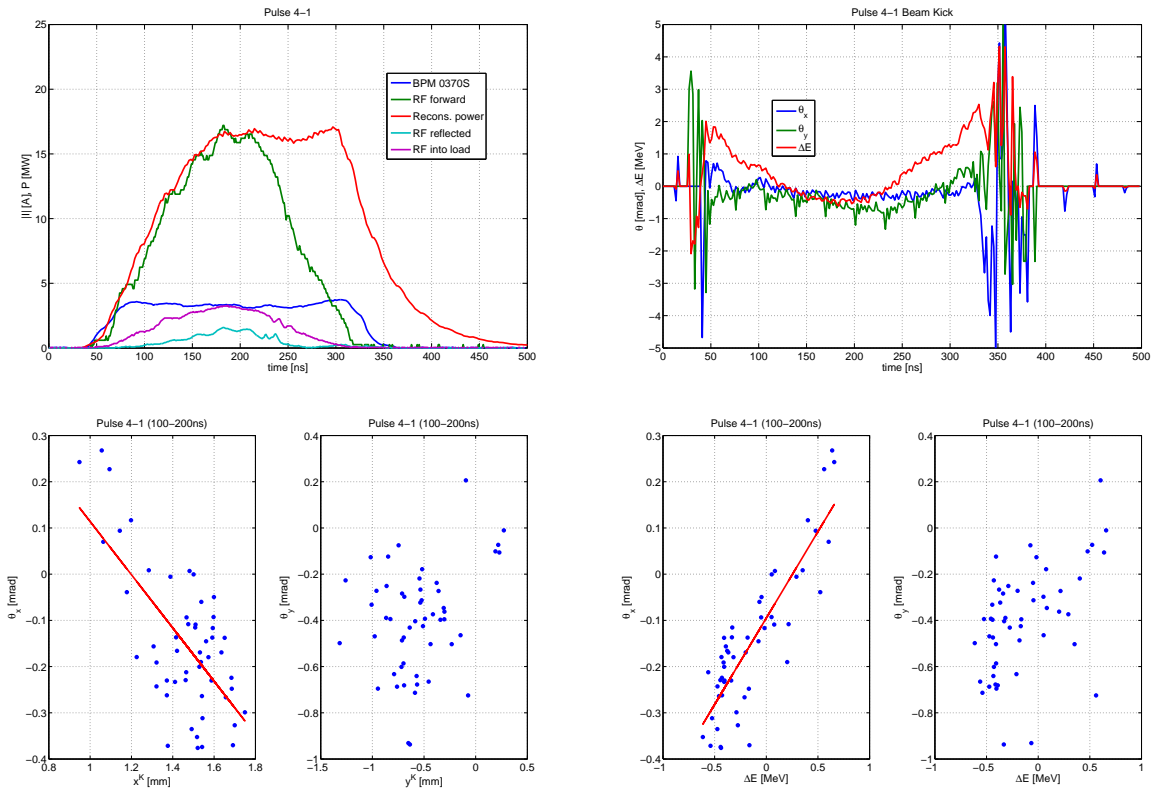


Figure 3: Plots of pulse number 4-1.

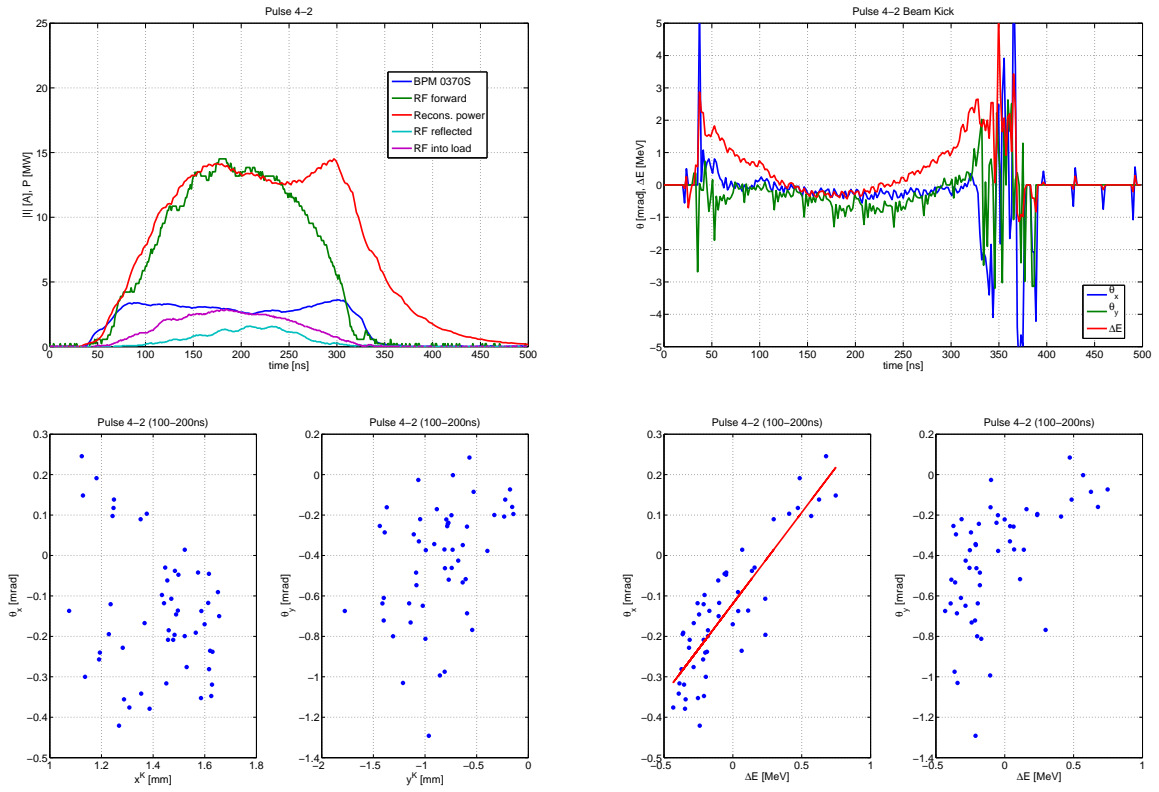


Figure 4: Plots of pulse number 4-2.

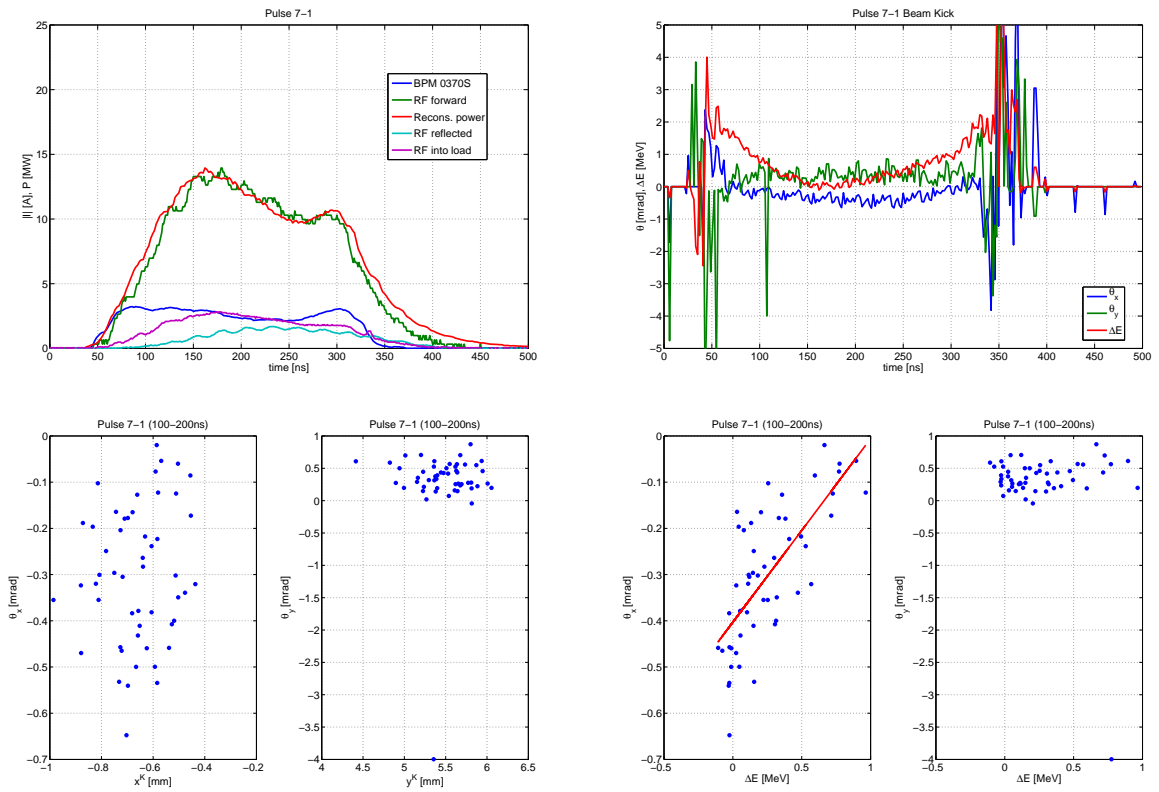


Figure 5: Plots of pulse number 7-1.

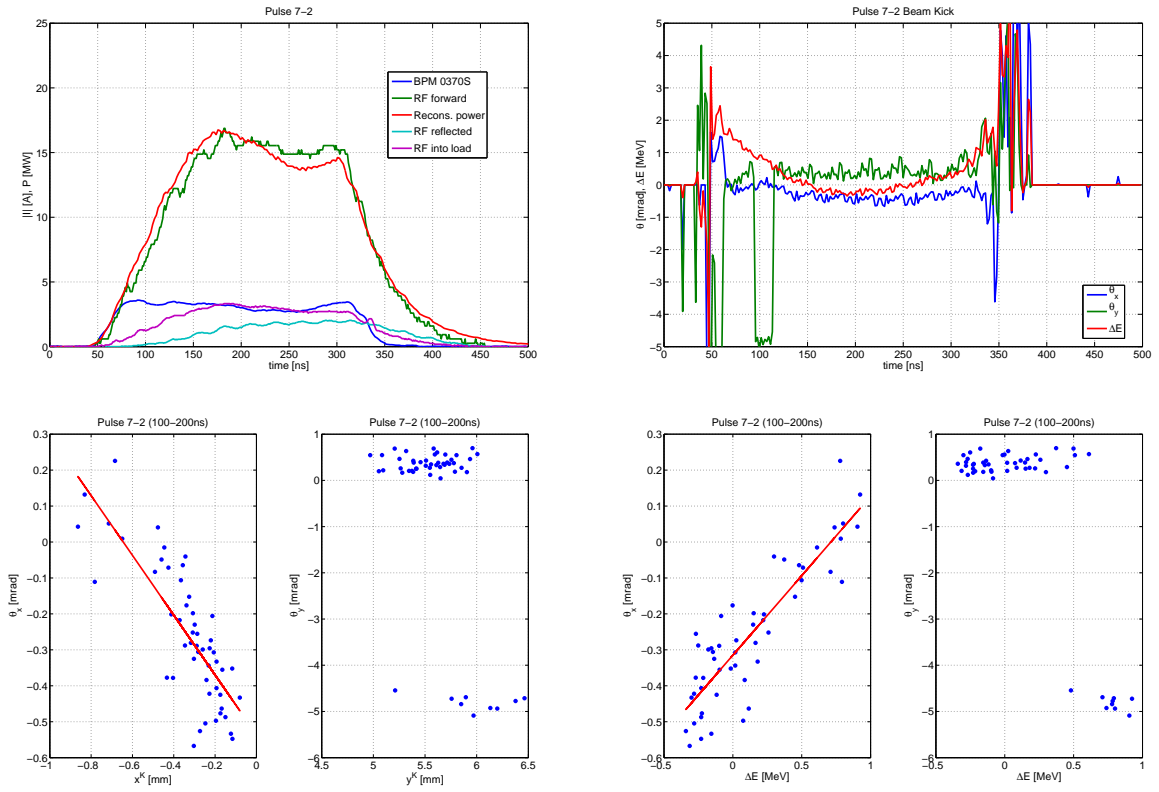


Figure 6: Plots of pulse number 7-2.

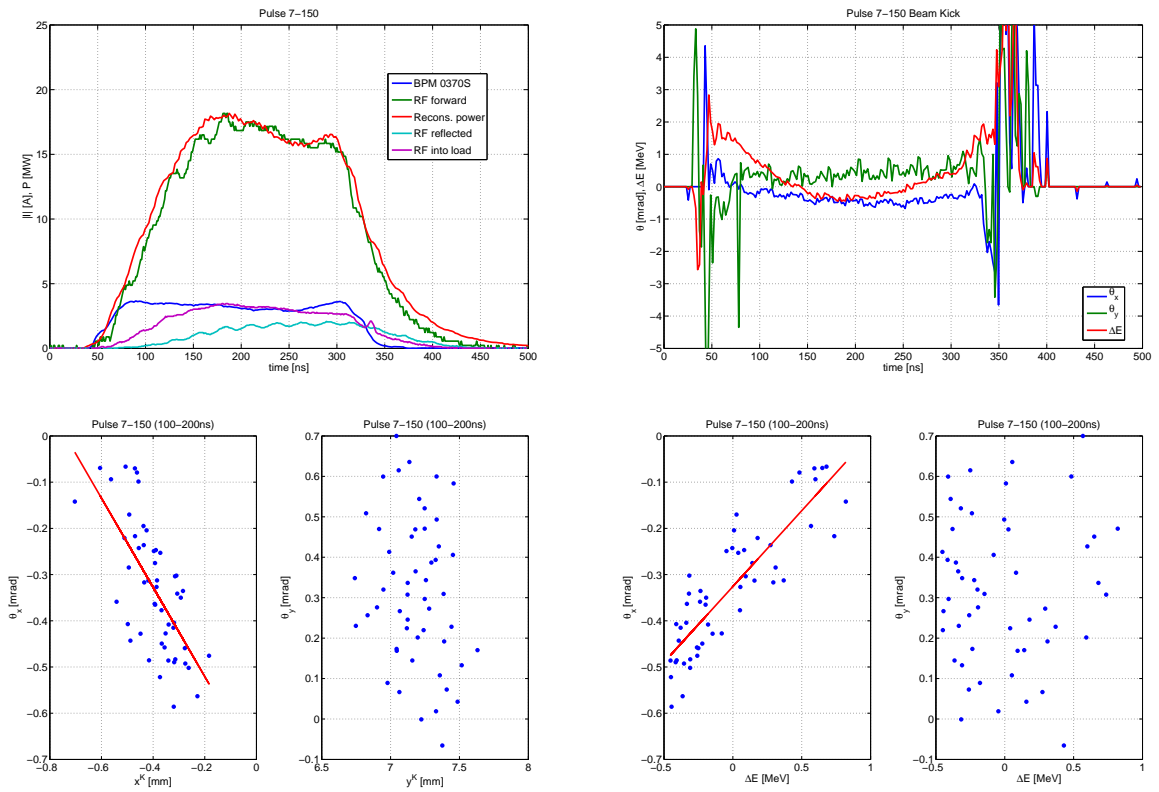


Figure 7: Plots of pulse number 7-150.

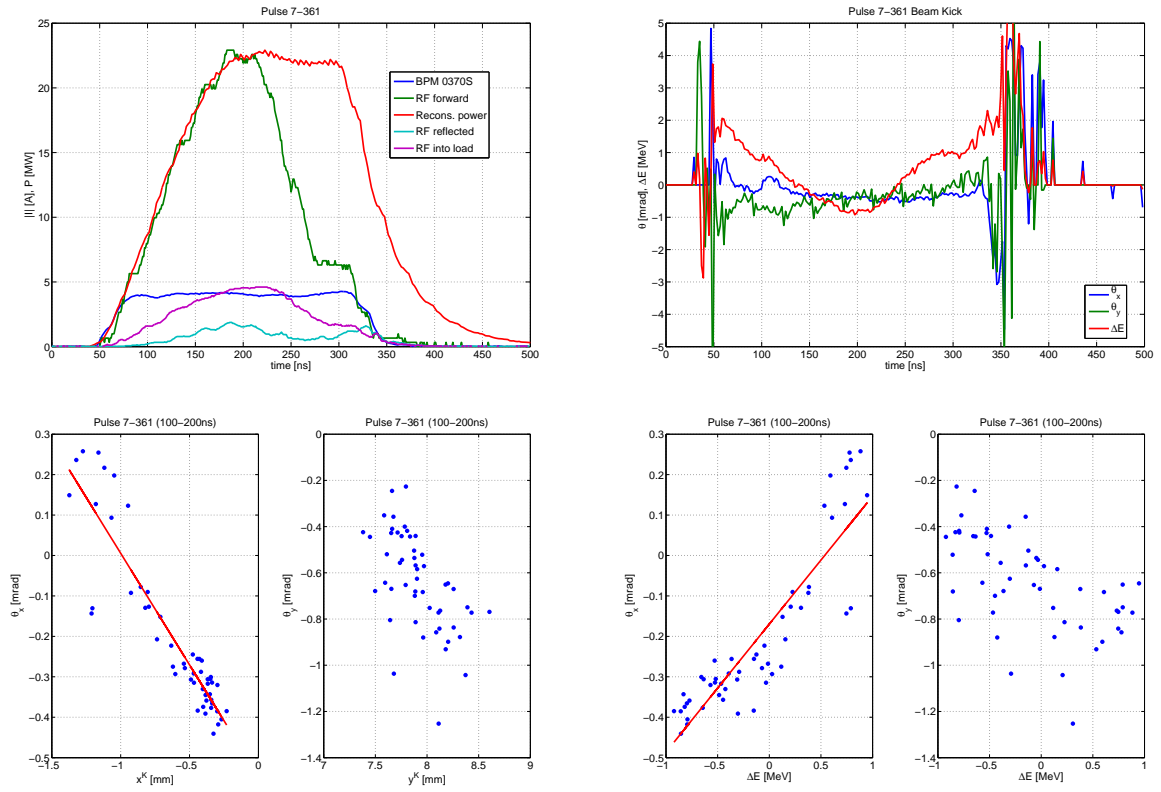


Figure 8: Plots of pulse number 7-361.

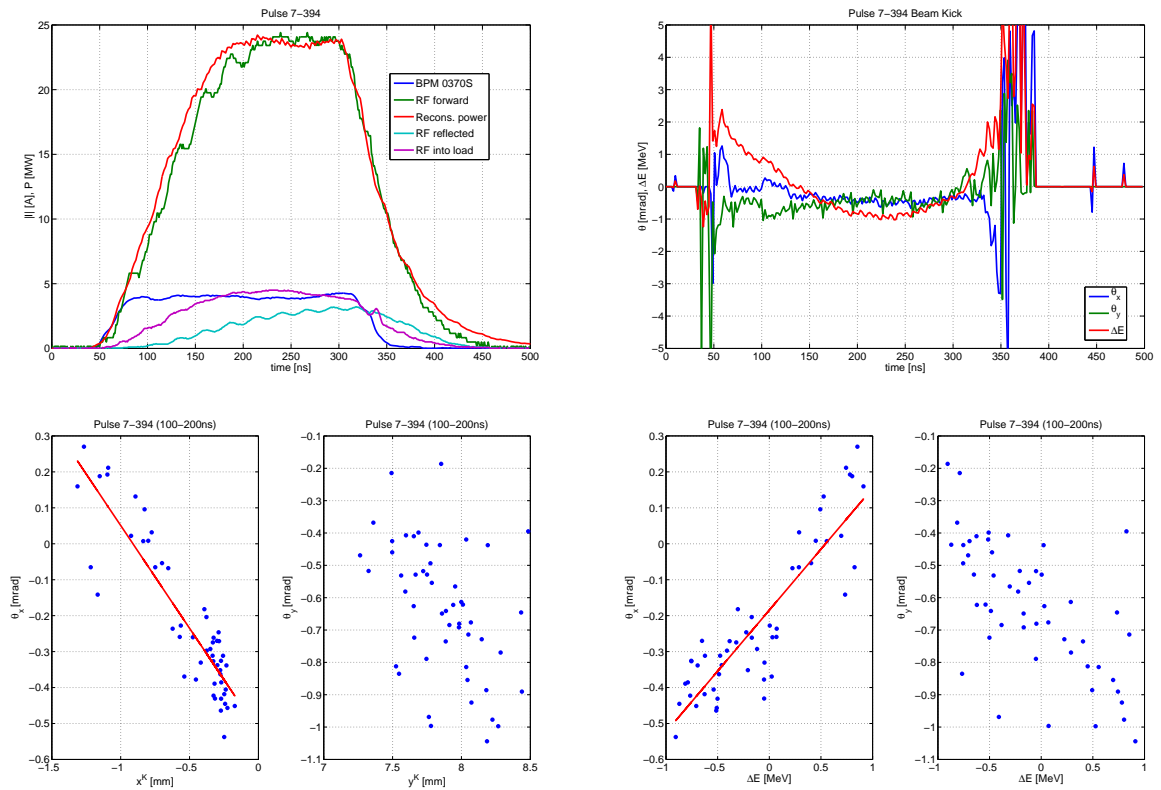


Figure 9: Plots of pulse number 7-394.

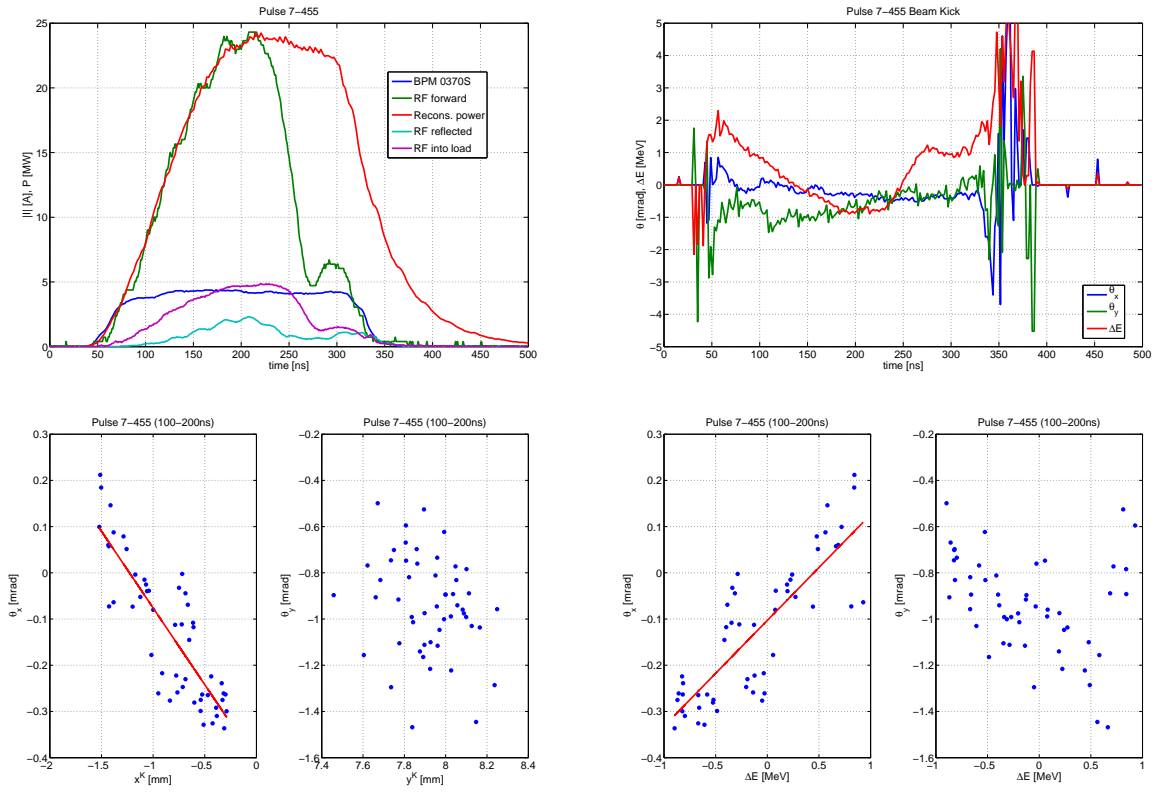


Figure 10: Plots of pulse number 7-455.

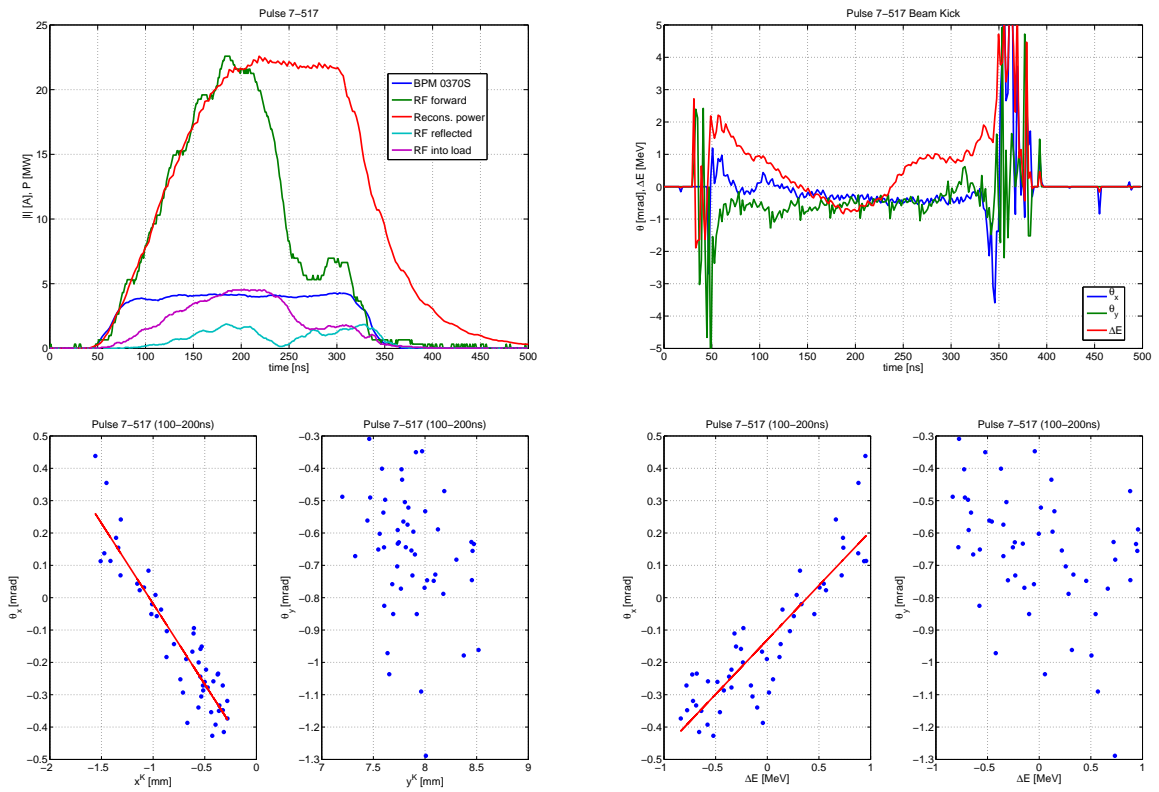
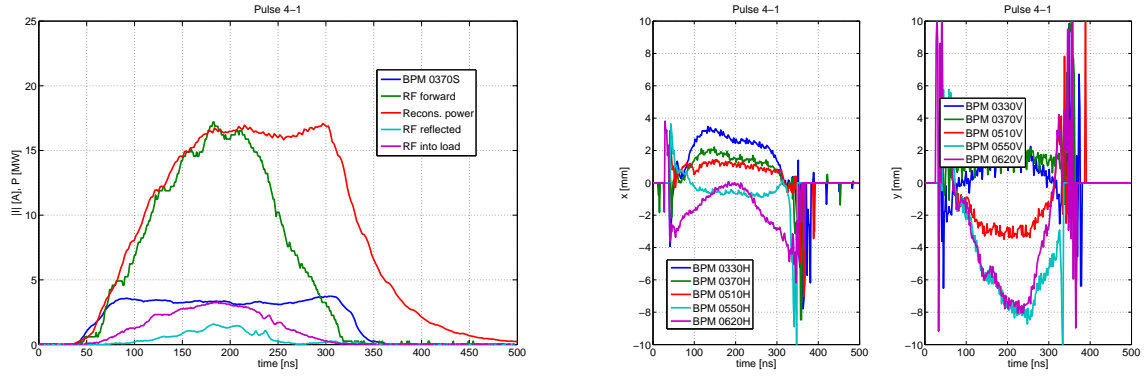


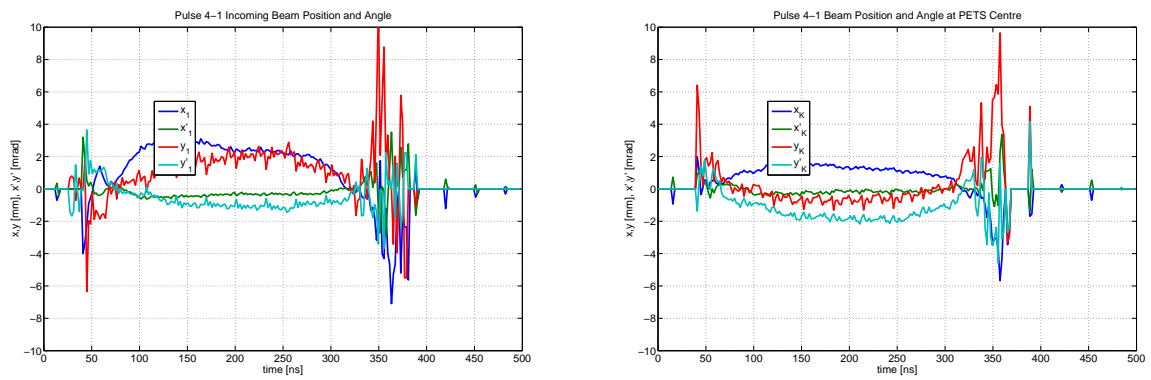
Figure 11: Plots of pulse number 7-517.

## D Extended Data Plots

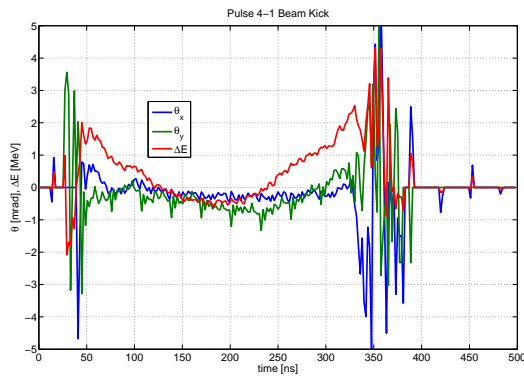
The plots for each pulse are divided over 4 figures. The first figure contains plots of the PETS output RF power, beam intensity, beam position and kick. The second figure contains correlation plots between beam kick and beam position, beam angle, beam intensity, RF power or beam energy loss. The data in these plots is from the flat top only. The third and fourth figure have the same plots as the second figure, but contain the data of the first halve and second halve of the flat top respectively.



(a) Beam current, measured RF power and reconstructed from the current (left) and beam position at the five BPMs (right).

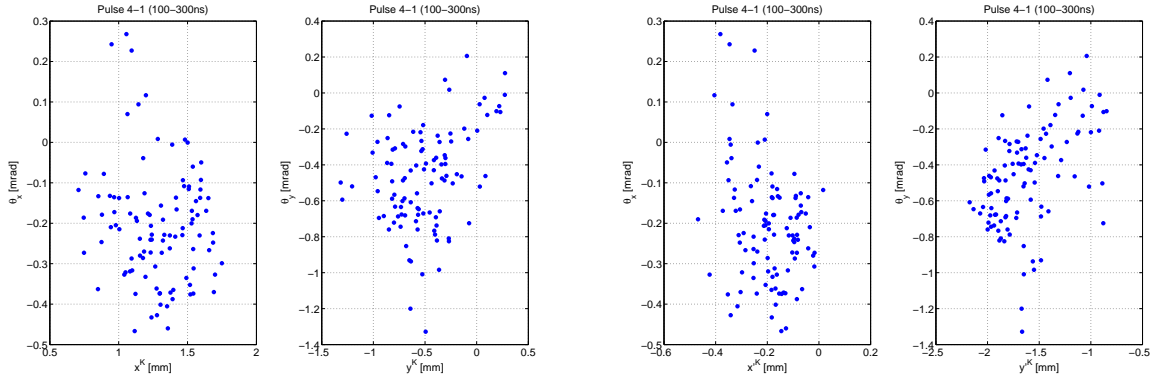


(b) Position of the incoming beam at BPM 1 (left) and at the PETS centre (right).

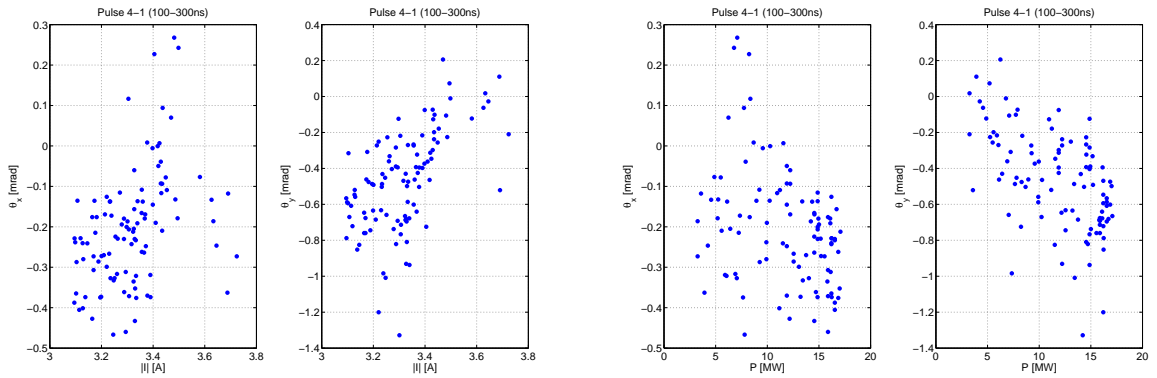


(c) Estimated beam kick and energy loss.

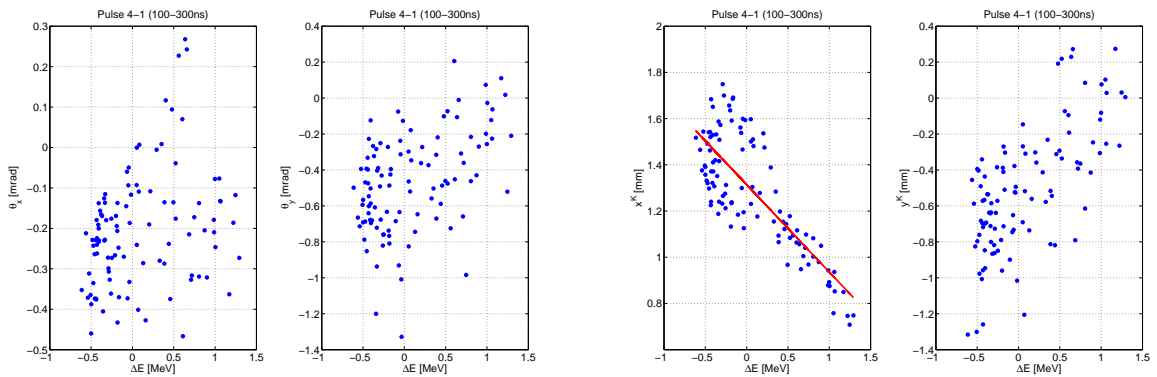
Figure 12: Plots of pulse number 4-1.



(a) Beam kick versus position (left) and angle (right).

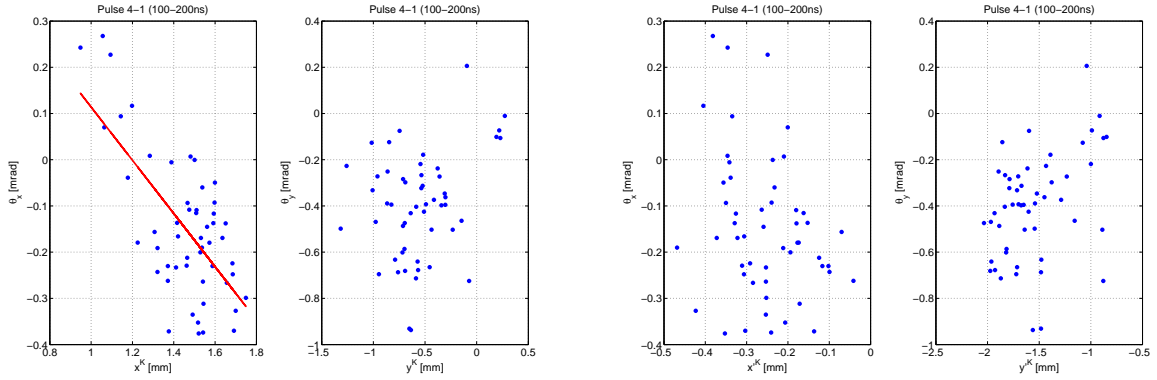


(b) Beam kick versus current (left) and RF power (right).

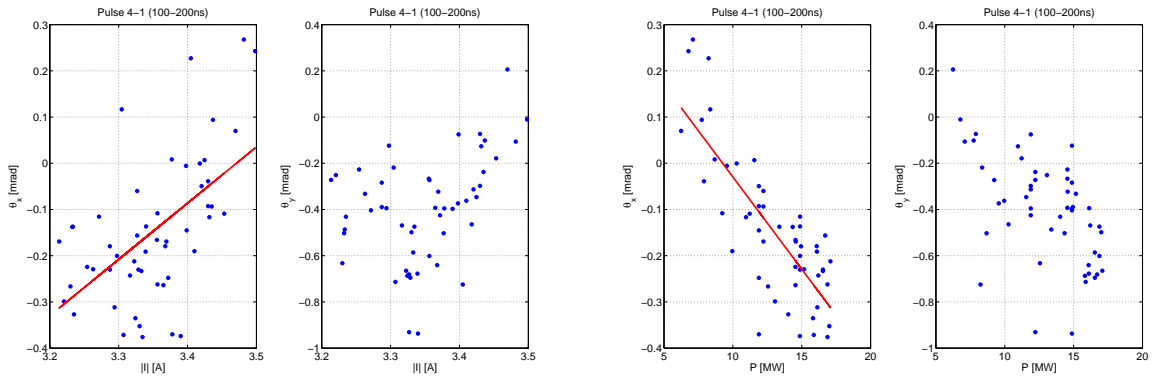


(c) Beam kick versus energy loss (left) and beam position versus energy loss (right).

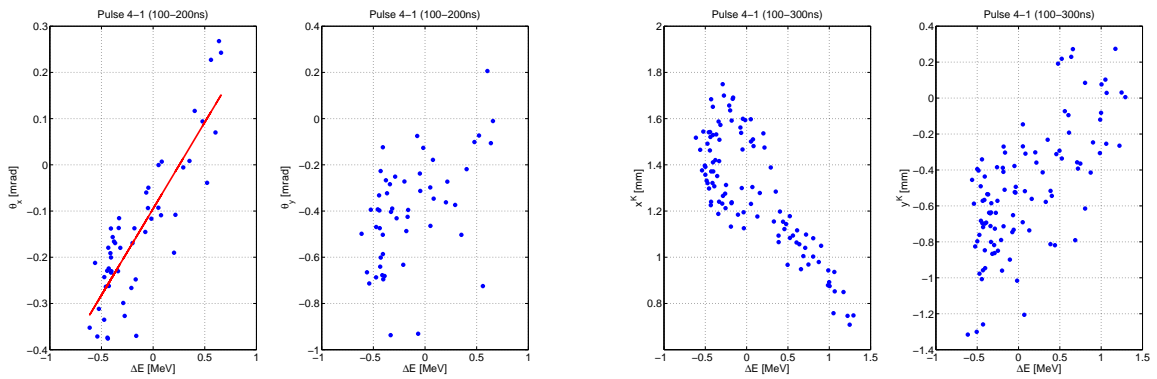
Figure 13: Correlation plots for pulse number 4-1. The plots contain only data from the beam current flat top.



(a) Beam kick versus position (left) and angle (right).

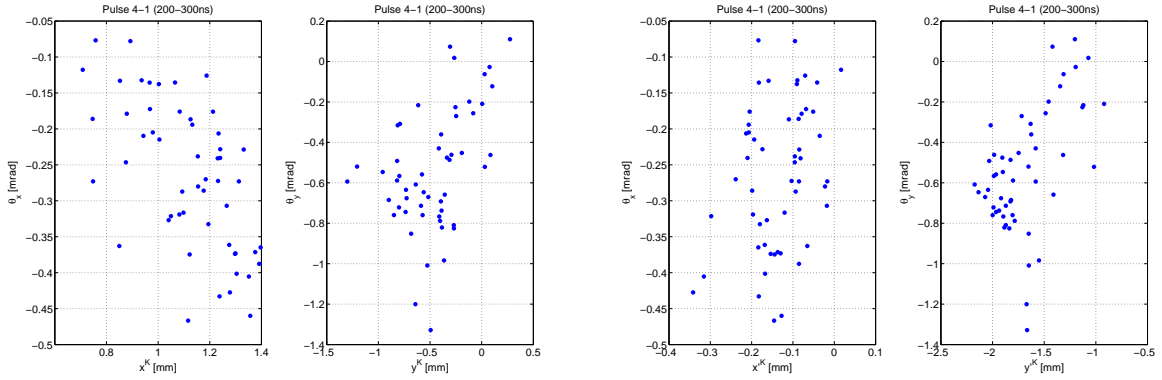


(b) Beam kick versus current (left) and RF power (right).

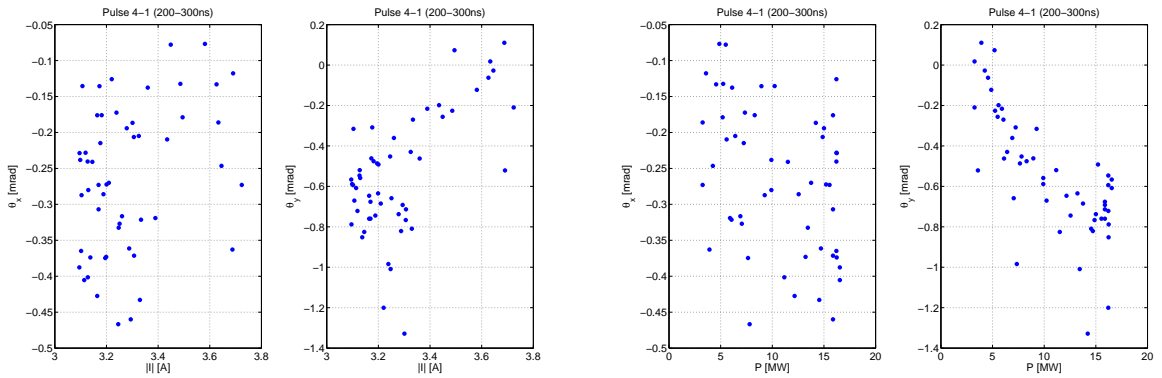


(c) Beam kick versus energy loss (left) and beam position versus energy loss (right).

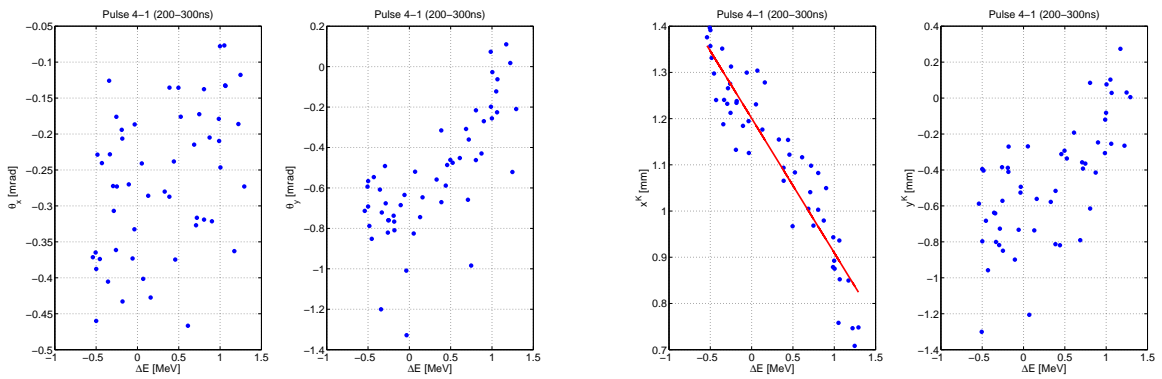
Figure 14: Correlation plots for pulse number 4-1. The plots contain only data from the beam current flat top between 100 and 200 ns.



(a) Beam kick versus position (left) and angle (right).

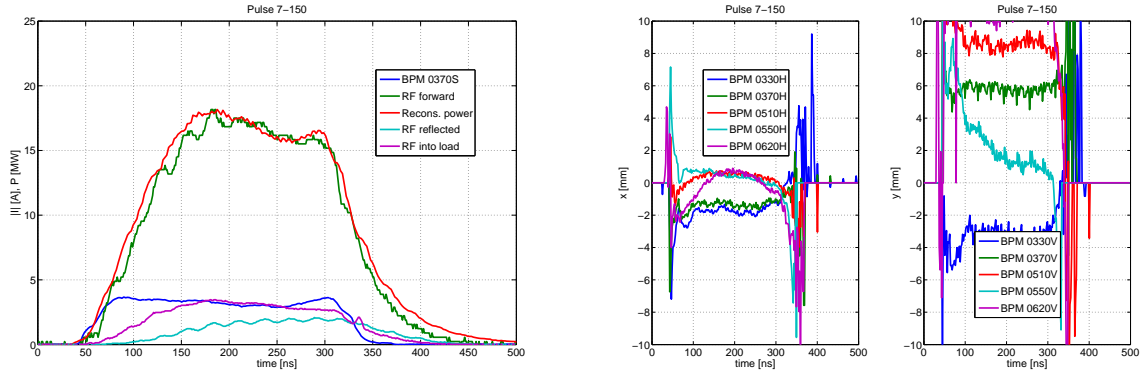


(b) Beam kick versus current (left) and RF power (right).

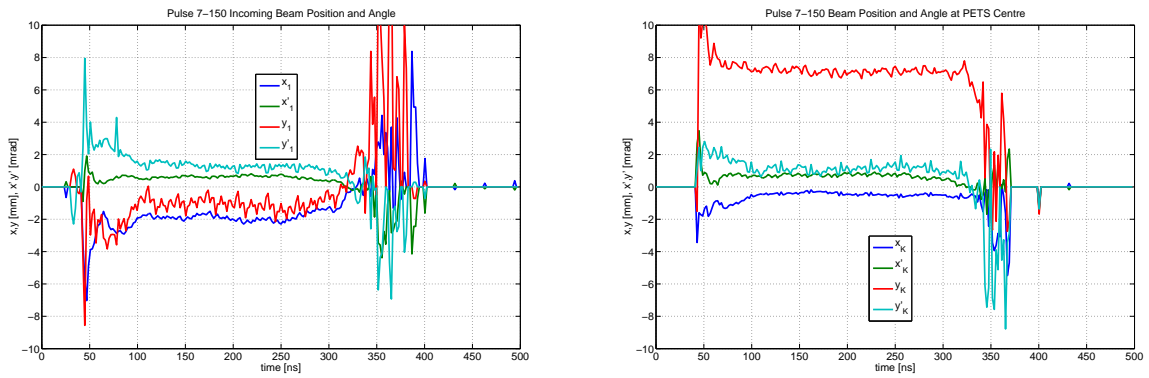


(c) Beam kick versus energy loss (left) and beam position versus energy loss (right).

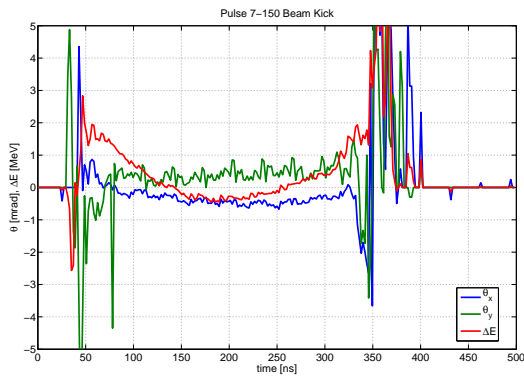
Figure 15: Correlation plots for pulse number 4-1. The plots contain only data from the beam current flat top between 200 and 300 ns.



(a) Beam current, measured RF power and reconstructed from the current (left) and beam position at the five BPMs (right).

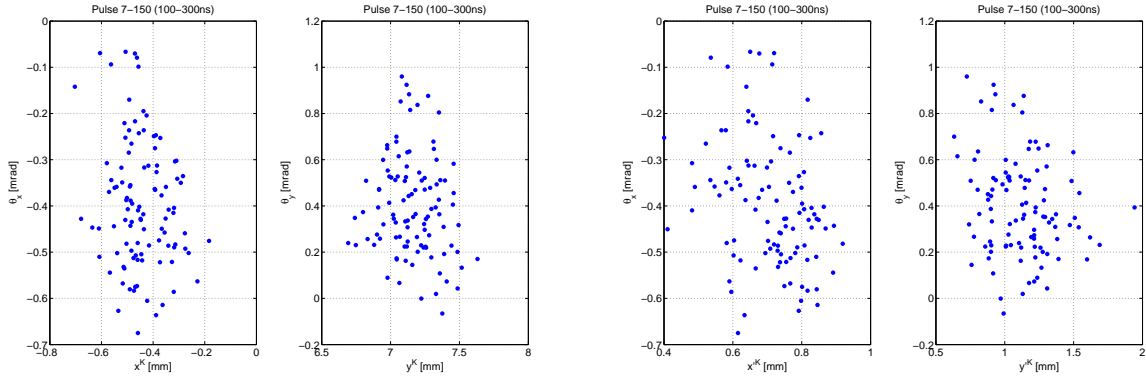


(b) Position of the incoming beam at BPM 1 (left) and at the PETS centre (right).

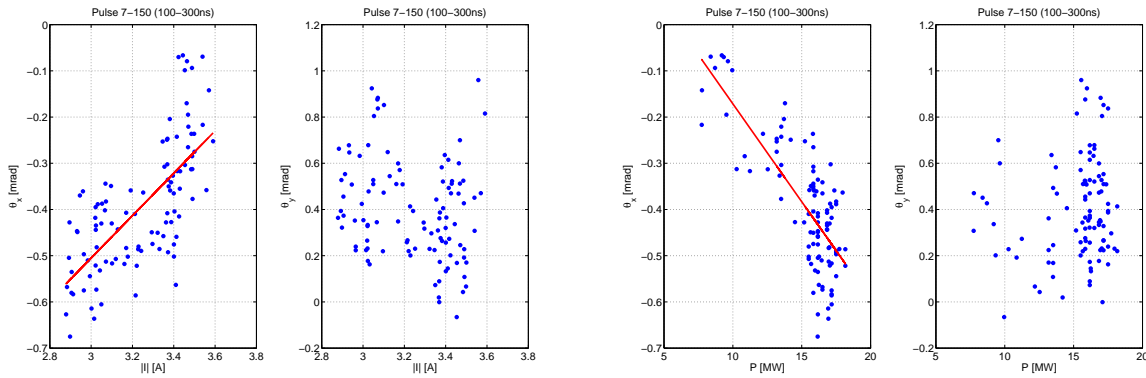


(c) Estimated beam kick and energy loss.

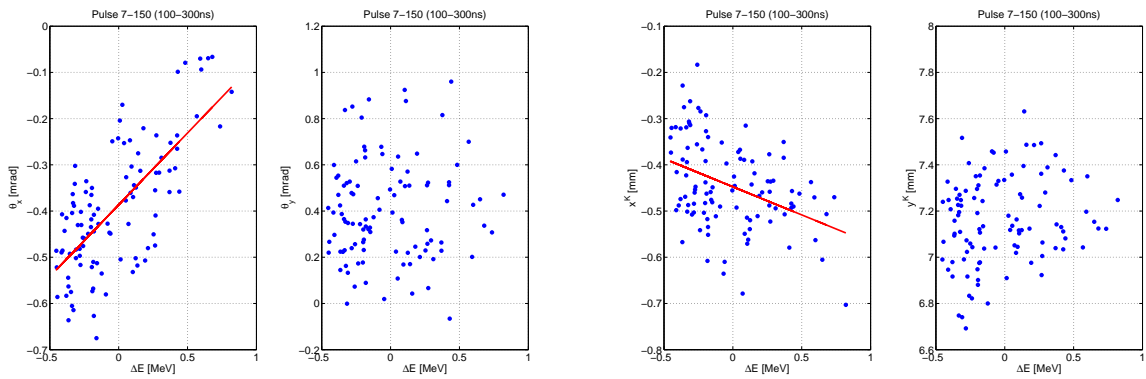
Figure 16: Plots of pulse number 7-150.



(a) Beam kick versus position (left) and angle (right).

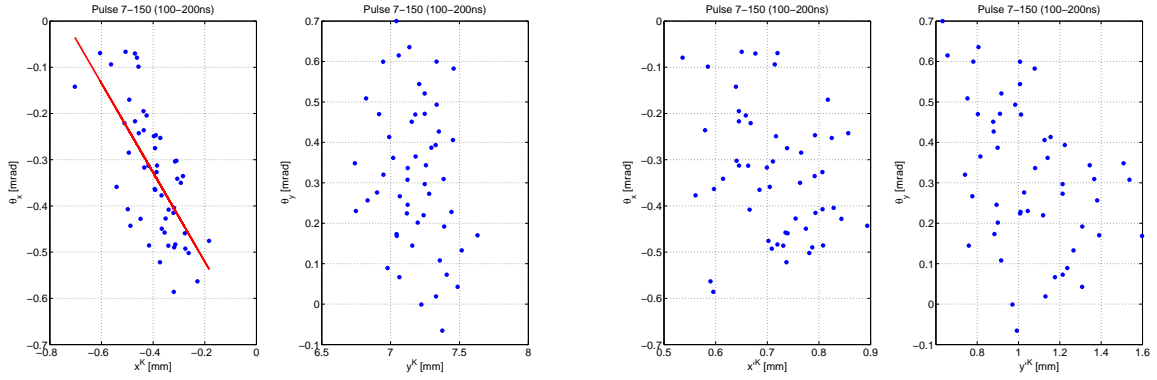


(b) Beam kick versus current (left) and RF power (right).

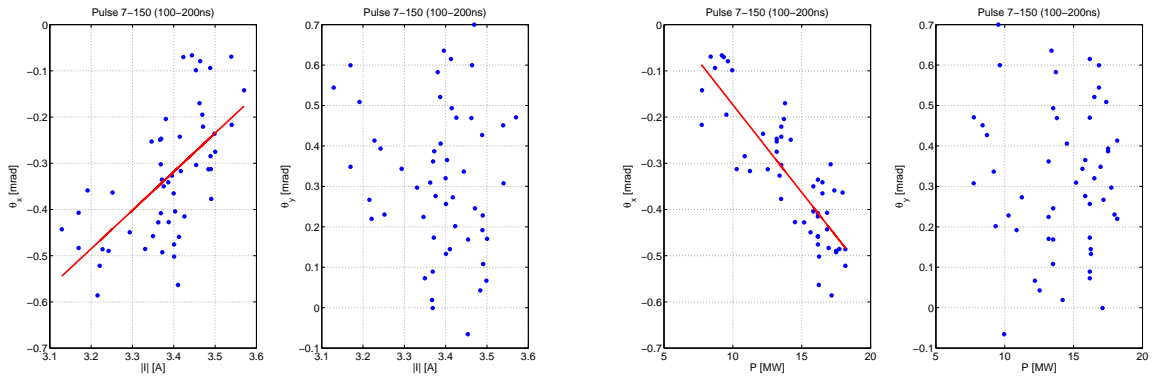


(c) Beam kick versus energy loss (left) and beam position versus energy loss (right).

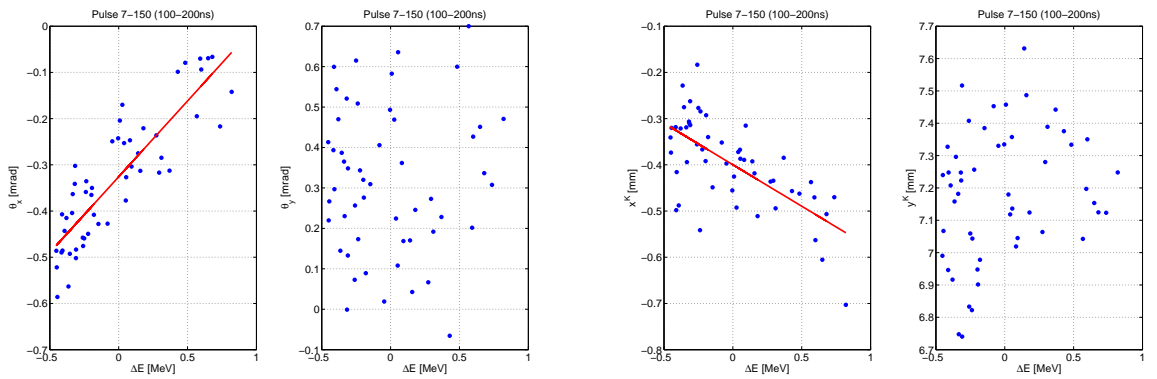
Figure 17: Correlation plots for pulse number 7-150. The plots contain only data from the beam current flat top.



(a) Beam kick versus position (left) and angle (right).

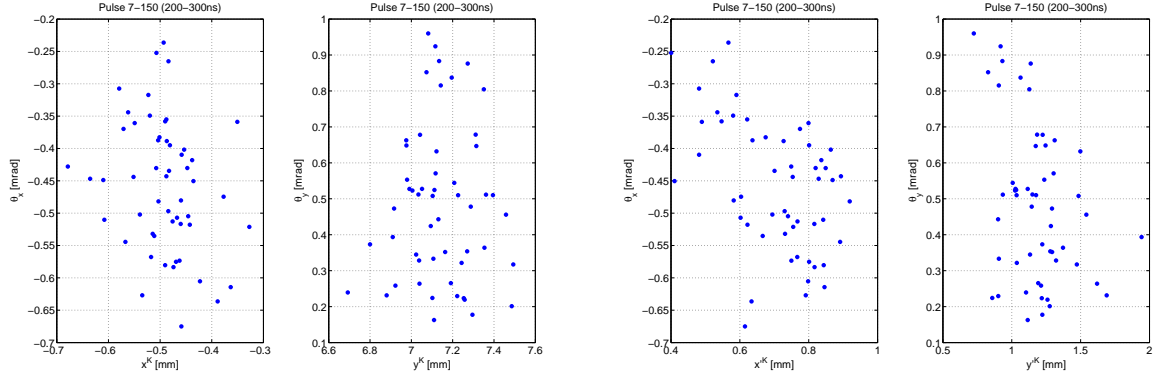


(b) Beam kick versus current (left) and RF power (right).

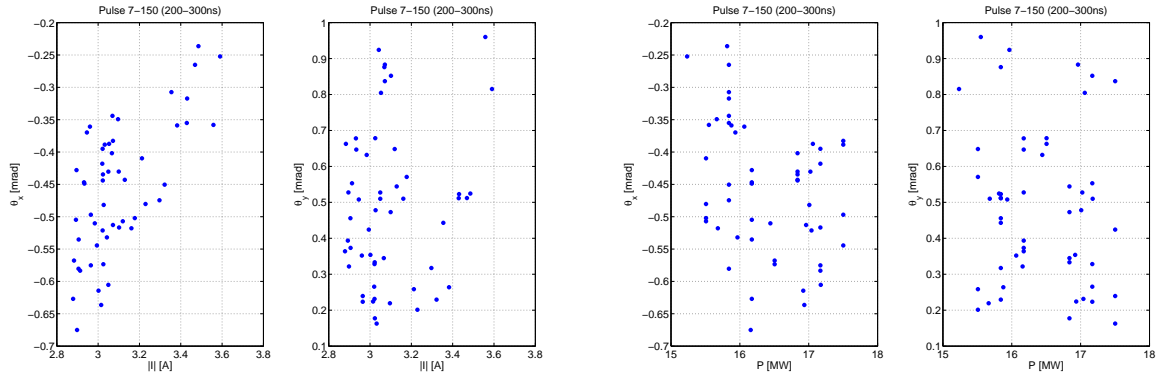


(c) Beam kick versus energy loss (left) and beam position versus energy loss (right).

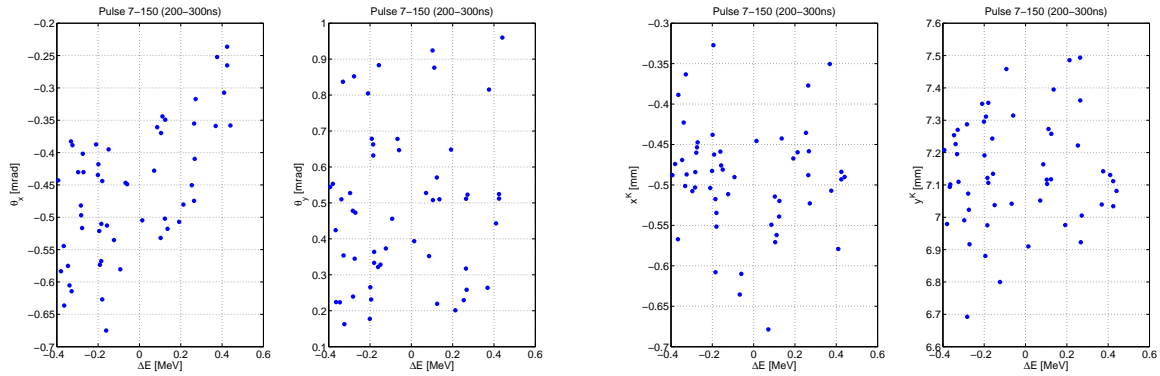
Figure 18: Correlation plots for pulse number 7-150. The plots contain only data from the beam current flat top between 100 and 200 ns.



(a) Beam kick versus position (left) and angle (right).



(b) Beam kick versus current (left) and RF power (right).



(c) Beam kick versus energy loss (left) and beam position versus energy loss (right).

Figure 19: Correlation plots for pulse number 7-150. The plots contain only data from the beam current flat top between 200 and 300 ns.